Published in final edited form as:
Ultrasound Med Biol. 2014 October ; 40(10): 2404–2414. doi:10.1016/j.ultrasmedbio.2014.04.013.

Monitoring and Staging Abdominal Aortic Aneurysm (AAA) Disease with Pulse Wave Imaging (PWI)

Sacha D. Nandlall[a], **Monica P. GoldKlang**[a], **Aubrey Kalashian**[a], **Nida A. Dangra**[a], **Jeanine M. D'Armiento**[a], and **Elisa E. Konofagou**[a,*]

Sacha D. Nandlall: sn2480@columbia.edu

[a]Columbia University, New York, NY, USA

Abstract

The Abdominal Aortic Aneurysm (AAA) is a silent and often deadly vascular disease caused by the localized weakening of the arterial wall. Previous work has shown that local changes in wall stiffness can be detected with Pulse Wave Imaging (PWI), which is a noninvasive technique for tracking the propagation of pulse waves along the aorta at high spatial and temporal resolutions. This study aims at assessing the capability of PWI to monitor and stage AAA progression in a murine model of the disease. ApoE/TIMP-1 knockout mice (N = 18) were given angiotensin II for 30 days via subcutaneously implanted osmotic pumps. The suprarenal sections of the abdominal aortas were imaged every 2-3 days after implantation using a 30 MHz Visualsonics Vevo 770 with 115 μm lateral resolution. Pulse wave propagation was monitored at an effective frame rate of 8 kHz by using retrospective electrocardiogram (ECG) gating and by performing 1-D cross-correlation on the radio-frequency (RF) signals to obtain the displacements induced by the waves. In normal aortas, the pulse waves propagated at constant velocities (2.8±0. 9 m/s, r^2 = 0.89±0.11), indicating that the composition of these vessels was relatively homogeneous. In the mice that developed AAAs (N = 10), the wave speeds in the aneurysm sac were 45% lower (1.6±0.6 m/s) and were more variable (r^2 = 0.66±0.23). Moreover, the wave-induced wall displacements were at least 80% lower within the sacs compared to the surrounding vessel. Finally, in mice that developed fissures (N = 5) or ruptures (N = 3) at the sites of their AAA, higher displacements directed out of the lumen and with no discernible wave pattern (r^2 < 0.20) were observed throughout the cardiac cycle. These findings show that PWI can be used to distinguish normal murine aortas from aneurysmal, fissured, and ruptured ones. Hence, PWI could potentially be used to monitor and stage human aneurysms by providing information complementary to standard B-modes.

*Corresponding Author: Elisa Konofagou, Department of Biomedical Engineering, Columbia University, 1210 Amsterdam Ave, ET 351, MC 8904, New York, NY 10027;, ek2191@columbia.edu; Phone, +1 212 342 1612.

Keywords

abdominal aortic aneurysm (AAA); fissure; high-frequency imaging; mice; motion estimation; normalized cross-correlation (NCC); pulse wave velocity (PWV); regional pulse wave; rupture; speckle tracking; ultrasound imaging

Introduction

The Abdominal Aortic Aneurysm (AAA) is a common vascular disease characterized by a localized ballooning or dilation of the abdominal section of the aorta, often as a result of a localized weakness in the vessel wall (Crawford et al., 2003). Depending on the age group, AAAs are estimated to occur in 1.3% to 12.5% of men and up to 5.2% of women, with prevalence rising in older age groups (Go et al., 2013). The leading cause of AAA-induced death is severe internal bleeding following a sudden rupture of the vessel wall within the sac of the aneurysm. Even with immediate medical attention, over 85% of ruptured AAAs eventually prove fatal, and approximately half of those afflicted die even before reaching the hospital (Patterson et al., 2008; Forsdahl et al., 2009). In the developed world, ruptured AAAs are a leading cause of death in males 65-85 years old and are responsible for up to 2% of deaths in the entire population (Sakalihasan et al., 2005; Urbonavicius et al., 2008), including over 10,000 deaths annually in the United States (Murphy et al., 2013) as well as over 7,000 deaths annually in England and Wales (Stather et al., 2013).

AAAs are typically diagnosed with noninvasive imaging modalities such as Magnetic Resonance Imaging (MRI), Computerized Tomography (CT), and 2-D ultrasound B-mode images (Crawford et al., 2003; Sakalihasan et al., 2005). However, screening for AAAs is challenging because most patients are asymptomatic until the aneurysm ruptures (Sakalihasan et al., 2005; Patterson et al., 2008) and relatively few definitive risk factors have been identified (Manning et al., 2002; Crawford et al., 2003). As a result, only the USA, the UK, and Sweden have implemented standardized AAA screening procedures nationally (Stather et al., 2013). Moreover, even when an AAA is detected, the options for treating it are currently open surgery or endovascular repair (Brewster et al., 2003). Both of these procedures are only performed when the risk of AAA rupture is deemed to be greater than the risk of mortality from postoperative complications (Patterson et al., 2008), which is especially significant in the case of open surgery (Manning et al., 2002). The metric that is currently used for assessing risk of AAA rupture is the maximum transverse diameter of the aneurysm (Urbonavicius et al., 2008; Stather et al., 2013). Unfortunately, this criterion is a poor predictor of the actual likelihood of rupture (Vorp et al., 1998; Choksy et al., 1999; Brewster et al., 2003) and does not have a sound physical or theoretical basis (Allison et al., 2008; McGloughlin and Doyle, 2010). This means that currently, many small AAAs that are deemed too small to treat end up rupturing regardless, and several patients with large but stable AAAs are subjected to unnecessary surgery.

A better means of assessing rupture risk is to measure localized changes in the material and mechanical properties of the vessel. Such parameters play a greater role than diameter in determining whether or not a rupture occurs, notably because their values change depending on the amounts of collagen and elastin present in the vessel wall (Lasheras, 2007; Haskett et

al., 2010). In particular, multiple clinical studies have established that arterial stiffness as a biomarker of all-cause and cardiovascular disease-related mortality (Hamilton et al., 2007; Zoungas and Asmar, 2007; Adji et al., 2011). In the clinic, carotid-femoral Pulse Wave Velocity (PWV) is currently the gold standard metric of arterial stiffness (Sutton-Tyrrell et al., 2005; Laurent et al., 2006; Nemes et al., 2011). Every cardiac cycle, the ejection of blood from the left ventricle of the heart sends a pulse wave propagating throughout the arterial tree, which gives rise to the natural pulsation of the arteries and induces a displacement wave in the vessel walls (Fung, 1996). The velocity of this wave, i.e. the PWV, is mathematically linked to the radial stiffness of the vessel via the Moens-Korteweg equation (Moens, 1877; Korteweg, 1878), which is derived from Newton's second law and states that the Young's modulus of the vessel wall is proportional to the square of the PWV (under certain simplifying assumptions, including a homogeneous, perfectly cylindrical vessel as well as small wall displacements relative to the baseline vessel diameter). As with arterial stiffness, PWV has been shown to be an effective biomarker for several diseases, particularly in hypertensive patients (Lehmann, 1999; Mitchell, 2009).

Various methods have been used to image pulse wave propagation, including pressure catheterization (Segers et al., 2005), phase contrast Magnetic Resonance Imaging (MRI) (Kraft et al., 2001; Macgowan et al., 2002), and pulsed Doppler imaging (Hartley et al., 1997; Eriksson et al., 2002; Rabben et al., 2004). The most common method is applanation tonometry (Lehmann, 1999; Laurent et al., 2006), in which PWV is computed by measuring the time delay between the pulse pressure waveforms at two different points in the circulation (typically the carotid and femoral arteries), and dividing the estimated distance between these two points by the measured time delay. However, because this technique only provides an average, global PWV and can be affected substantially by variations in the estimated arterial path length (Sugawara et al., 2010), it is unsuitable for measuring highly localized changes in stiffness that would indicate the onset of an aneurysm.

Pulse Wave Imaging (PWI) is a noninvasive, ultrasound-based technique for visualizing and tracking the propagation of pulse waves along the arterial wall at high spatial and temporal resolutions. PWI has been validated *in silico* using simulations (Shahmirzadi and Konofagou, 2012), *in vitro* using phantoms (Vappou et al., 2010; Shahmirzadi et al., 2013), *ex vivo* with canine aorta (Shahmirzadi et al., 2013), *in vivo* with mice (Fujikura et al., 2007; Pernot et al., 2007; Luo et al., 2009), and clinically in humans (Luo et al., 2012; Li et al., 2013). The high resolution of PWI means that it can provide localized maps of PWV, thereby allowing for the identification of subtle changes in the pulse wave propagation patterns as well as regional variations in vessel wall stiffness. This capability could allow PWI to identify emerging abnormalities in the vessel that act as precursors to aneurysm formation and are not visible or easily detectable with standard imaging modalities such as ultrasound B-modes.

The objective of this study is to investigate the feasibility of using PWI to monitor and stage the progression of AAAs in vivo. To this end, a murine model of gradual AAA development based on the infusion of angiotensin II in ApoE/TIMP-1 knockout mice was used in this study (Lemaître, 2002; Manning et al., 2002; Luo et al., 2009). Although PWI can be applied in humans, using a murine model enables disease progression to be monitored over

its entire duration at many closely spaced time-points. Additional advantages of murine aneurysms for the purposes of this study are that they can be instigated in a controlled fashion, require significantly less time to develop (several weeks in mice compared to years in humans), and can be imaged at higher resolutions (since the required imaging depth is smaller in mice, there is less attenuation, and hence higher frequencies and frame rates can be used). In the murine angiotensin II AAA model, three distinct phases of disease progression can be observed: first, the appearance of a fissure in the aortic wall; second, the development of the aneurysm with a sac and possibly an intraluminal thrombus (Thubrikar et al., 2003; Wilson et al., 2013), usually in the anterior wall near the superior mesenteric or coeliac arteries (Lemaître, 2002; Manning et al., 2002); and third, the rupture of the aneurysm. In the existing literature (de Prophetis et al., 1959; Klevay, 2000), aneurysms are typically defined as a localized increase of 50% or more in the inner diameter of the vessel, while the terms “fissure” and “rupture” refer to an opening in the vessel wall in a region that eventually develops an aneurysm (fissure) or previously contained an aneurysm (rupture). Previous work by Luo et al. (2009) demonstrated the feasibility of using PWI to distinguish normal aortas from aneurysmal ones qualitatively in the murine AAA model, but did not examine the progression of the disease between the administration of angiotensin II and the appearance of aneurysms. Hence, this study will assess the capability of PWI to distinguish between all four possible stages of the murine aorta throughout AAA disease progression: normal, fissured, aneurysmal, and ruptured.

Materials and Methods

Animal Model

All procedures performed in this study were approved by the Institutional Animal Care and Use Committee (IACUC) of Columbia University (protocol AC-AAAG4951). Eighteen (N = 18) male ApoE/TIMP-1 knockout mice were infused with angiotensin II (Sigma-Aldrich, A9525, St. Louis, MO, USA) for 30 days via subcutaneously implanted osmotic pumps (Durect, Alzet Model 2004, Cupertino, CA, USA). Seven (N = 7) of the mice received a baseline dose of 2.2 mg/kg/day (milligrams of angiotensin II per kilogram of body mass per day), while the other eleven (N = 11) mice were given a double dose of 4.4 mg/kg/day. This animal model has been employed previously by other studies (Lemaître, 2002; Manning et al., 2002; Luo et al., 2009), although the angiotensin II dose used in other works is typically only 1.44 mg/kg/day. In this study, higher doses were used in order to instigate more rupture events, which occur less frequently at standard dosage levels.

Setup

A block diagram of the PWI setup is shown in Figure 1. All imaging was done using a Vevo 770 ultrasound imager (Visualsonics, Toronto, ON, Canada). Imaging was performed over a 12 mm by 12 mm field of view using an RMV-707B single-element probe, which had a focal length of 12.7 mm, a center frequency of 30 MHz, a −3 dB bandwidth of 15-45 MHz, an axial resolution of 55 μm, and a lateral resolution of 115 μm.

During imaging, each mouse was anesthetized with a mixture of 2% isoflurane (AErrane, Baxter Healthcare, Deerfield, IL, USA) and pure oxygen (Tech Air, White Plains, NY,

USA), administered via inhalation using an isoflurane vaporizer (Model 100, SurgiVet, Waukesha, WI, USA). The mouse was then placed in a supine position on a heated platform to maintain its body temperature at approximately 37°C. The hair over the areas being imaged was removed with a shaver and depilatory cream. Degassed ultrasound gel (Aquasonic 100, Parker Laboratories, Fairfield, NJ, USA) was utilized as a coupling medium; care was exercised to avoid the formation of air bubbles in the gel.

Throughout the acquisition, the electrocardiogram (ECG) for each mouse was monitored with a THM-100 ECG monitor (Indus Instruments, Webster, TX, USA). The radio-frequency (RF) signals from the Vevo 770 as well as the ECG signal from the THM-100 monitor were recorded using a Gage CompuScope 14200 data acquisition card (Dynamic Signals, Montreal, QC, Canada) at a sampling frequency of 200 MHz and a resolution of 14 bits per sample.

Imaging Protocol

Prior to each PWI acquisition, blood flow was measured at two points in the middle of the lumen using the Pulse Wave (PW) Doppler mode of the Vevo 770. PW Doppler measurements were also recorded within the sacs of aneurysms, as well as in the region surrounding the vessel wall at the sites of ruptures (i.e. at locations where an aneurysm had previously existed), as illustrated in Figure 2. All PW Doppler measurements were performed at a Pulse Repetition Frequency (PRF) of 20 kHz and a 45 ° incidence angle.

PWI acquisitions for all mice were performed in the suprarenal section of the abdominal aorta. The Vevo 770 was operated in the manufacturer's ECG-gated Kilohertz Visualization (EKV) mode, in which the transducer is placed at a fixed lateral position and RF signals are acquired at a PRF of 8 kHz over several cardiac cycles. Each RF line is then co-registered with an R-wave (peak) in the ECG signal. Those RF lines that are closest in time to their respective peaks may be used to form the first frame ($t = 0$); similarly, the RF lines that immediately follow may be used to form the second frame ($t = 125\ \mu$s, i.e. the pulse repetition period), and so on for subsequent frames ($t = 250\ \mu$s, 375 μs, etc.). This process is repeated at successive lateral positions spaced 6.25 μm apart (less than the lateral resolution of the transducer) until the entire 12 mm field of view is covered. The lateral movement of the transducer during this process is controlled by an actuator within the body of the transducer (the transducer assembly itself does not move). An ECG-gated cine-loop of the aorta over an entire cardiac cycle was thus obtained for each acquisition. Since RF lines were acquired over several cardiac cycles at each position, the RF lines used to form the cine-loop were chosen to minimize lateral misalignment and give the clearest B-mode image.

For each mouse, PWI was performed one day prior to infusion as a control and every 2-3 days thereafter for 30 days, after which the mouse was sacrificed.

Disease Staging and Classification

As mentioned previously, there are four possible stages of disease progression in the murine angiotensin II AAA model: normal, fissured, aneurysmal, and ruptured (Thubrikar et al.,

2003; Wilson et al., 2013). In this study, each acquisition was classified into one of these four stages based on the associated B-mode image. An aneurysm was deemed to have occurred if a localized increase of 50% or more in the inner diameter of the vessel was present (de Prophetis et al., 1959; Klevay, 2000), while fissures and ruptures were defined as an opening in the vessel wall in a region that eventually developed an aneurysm (fissure) or previously contained an aneurysm (rupture). Figure 2 shows representative examples of B-modes associated with each disease stage. Note that the fissure classification can only be applied retroactively, once an aneurysm has formed at the same site.

Two additional techniques were used to verify the B-mode-based classifications for some of the acquisitions. First, at sites that appeared to contain fissures and ruptures, PW Doppler measurements of blood flow were recorded just outside the vessel wall, as shown in Figure 2. Second, for mice that survived the full 30 days of the study, histology was performed on the aorta shortly after the last acquisition. For these mice, the abdominal section of the aorta (from the diaphragm to just before the bifurcation) was removed, cleaned, and fixed in 4% (w/v) formaldehyde within the first hour after euthanasia. The fixed tissue was then embedded in paraffin and sectioned at a thickness of 10 μm. Several sections per tissue sample were stained with Hematoxylin and Eosin (H&E) and were visualized with an inverted microscope (IX-81, Olympus, Melville, NY, USA).

Displacement Estimation

All data were processed using MATLAB R2013a (The Mathworks, Natick, MA, USA). Since the vessel walls were oriented as parallel to transducer as possible, axial displacement alone was found to be sufficient to track the pulse waves in all cases. Axial displacement estimation was performed using a fast algorithm based on 1-D normalized cross-correlation, described in detail elsewhere (Luo and Konofagou, 2010). The correlation window size was set to 431 μm, which is approximately 7 acoustic wavelengths; according to previous studies (Walker and Trahey, 1995; Luo et al., 2009), window lengths between 5 and 10 wavelengths tend to produce displacements of optimal quality. The ofset between successive windows was 7.7 μm, i.e. exactly 1 sample (the smallest possible value). The estimated displacements were considered to be of acceptable quality if their associated correlation coefficients were at least 0.9.

The resulting axial wall displacements were normalized by multiplying them by the frame rate (8 kHz) and were then filtered in several steps. First, the effects of false peaks and jitter (Walker and Trahey, 1995) were compensated for by applying a 30 mm/s threshold to the wall velocities, which is equivalent to half a sample of displacement between two consecutive frames. Second, rigid body motion in each line (caused mainly by respiration) was corrected for by subtracting the mean wall displacement over a 1 mm stationary segment at least 3 mm clear of the aorta, closer to the ventral end of the mouse (i.e. between the transducer and the aorta). Third, spatial noise such as misaligned lines and peak hopping errors were mitigated with a 5-point (575 μm) median filter. Finally, high-frequency spatial and temporal noise was reduced using a first-order Savitzky-Golay smoothing filter with a 2-D kernel size of 15 spatial points (1.725 mm) by 15 temporal points (1.875 ms). This filter type was chosen because it tends to preserve the location of local maxima and minima

(Savitzky and Golay, 1964), which are important features for the pulse wave tracking technique described in the next section.

Pulse Wave Tracking

To track the pulse wave, the peak of the wall displacement profile at each spatial location was found by determining the time at which the maximum wall displacement occurred (Chiu et al., 1991; Luo et al., 2009; Li et al., 2013). The foot was then defined as the time of occurrence of the smallest wall displacement before the peak. Finally, the 50% upstroke point was defined as the time between the foot and the peak at which the wall displacement was closest to the average of its values at the foot and peak (Luo et al., 2009; Li et al., 2013).

Plotting the 50% upstroke times along the length of the vessel wall (which was manually traced for each case using the first B-mode frame) and performing a linear regression on these time-distance pairs yields the PWV. The coeffcient of determination r^2 for this regression indicates how uniform the velocity of the pulse wave is over the wall segment that is being imaged.

In the animal model used in this study, aneurysms only form on the anterior side of the aorta (the top wall in all figures herein), typically near the superior mesenteric or coeliac arteries (Lemaître, 2002; Manning et al., 2002). For this reason, only the anterior wall was studied with PWI in this study.

Results

Example Case History for a Single Subject

In this study, a total of 142 PWI acquisitions (n = 142) were performed in eighteen mice (N = 18). However, before discussing the complete set of results, it is helpful to examine the case history of a single mouse by way of example. The mouse chosen for this analysis received 4.4 mg/kg/day of angiotensin II and was imaged in all four disease progression stages: normal on day 0 (the day before angiotensin II infusion), fissured on day 7, aneurysmal on day 13, and ruptured on day 18.

Figure 3 shows four sequences of still frames from the PWI cine-loops corresponding to each of the aforementioned disease stages and time points. Each sequence contains three frames that show the pulse wave entering (left), crossing (middle), and exiting (right) the field of view (see also Supplemental Video 1). The arrows indicate the location of the 50% upstroke point of the wave, while the overlay indicates displacement at the moment that the frame was captured. In each case, the lower and upper limits of the displacement color scale correspond respectively to the displacements at the foot and peak of the pulse wave.

Figure 4 shows the spatiotemporal displacement maps along the anterior (top) walls of the vessels for the sequences in Figure 3. The 50% upstroke markers as well as the piecewise linear regressions on these markers are superimposed on the spatiotemporal plots, along with the pulse wave velocities (the slopes of the lines) as well as the coefficients of determination (r^2) of the linear regressions.

Comparing the respective PWI sequences in Figure 3 and the spatiotemporal maps in Figure 4 shows that there are qualitative differences in the pulse wave propagation pattern associated with each disease stage. In the normal aorta (Figures 3a and 4a), the wave propagation is smooth and the PWV is relatively constant, as observed in previous work (Fujikura et al., 2007; Pernot et al., 2007; Luo et al., 2009). At the site of the fissure (Figures 3b and 4b), high displacements directed outwards from the lumen and with no discernible wave pattern ($r^2 = 0.06$) can be observed throughout the cardiac cycle; this is indicative of outward blood flow at the fissure site. In the aneurysm that developed six days later in the same location (Figures 3c and 4c), there is a marked decrease in displacement in the sac of the aneurysm compared to the normal vessel on either side; this pattern also agrees with observations in previous work (Luo et al., 2009). Finally, the rupture 5 days later (Figures 3d and 4d) shows a similar pattern to the fissure, with a high-displacement region at the rupture site and no discernible wave ($r^2 = 0.09$).

This example case therefore suggests that the aforementioned patterns of pulse wave propagation can be used to stage AAA development in this disease model, at least in a qualitative sense. This is indeed confirmed by the remainder of the results: similar patterns were observed in all of the other PWI acquisitions at each of the four AAA disease stages. Furthermore, in cases where the fissure or rupture was apparent on the B-mode during imaging (including the example case shown here), angle-corrected PW Doppler measurements indicated flow velocities of up to 40 cm/s at the site of the fissure or rupture, suggesting a high degree of blood leakage out of the vessel.

Statistical Analysis

Figure 5 shows the mean and standard deviation of PWV (Figure 5a) and r^2 (Figure 5b) in all PWI acquisitions, separated by disease stage. The fissure and rupture classifications are omitted from the PWV graph because the low value of r^2 for these disease stages indicates that there is no pulse wave to track at the sites of these abnormalities, which implies that it is not meaningful to define a “pulse wave velocity” in these cases. As shown in Figure 5a, PWV is on average 45% lower in aneurysms (1.6 ± 0.6 m/s, $n = 30$ acquisitions in $N = 10$ mice) than in normal aortas (2.8 ± 0.9 m/s, $n = 100$, $N = 18$). Similarly, Figure 5b shows that r^2 is highest in normal vessels (0.89 ± 0.11), lower in aneurysms (0.66±0.23), and lowest ($r^2 < 0.20$) in both fissures ($n = 7$, $N = 5$) and ruptures ($n = 5$, $N = 3$).

Significance levels as computed by the Kolmogorov-Smirnov test are also shown on both graphs in Figure 5. It can be seen that almost all pairs of categories are significant relative to one another with a p-value of less than 0.001; the sole exception is the fissures and ruptures pair, which displays a high degree of statistical similarity ($p = 0.87$). The Kolmogorov-Smirnov test was used instead of a standard Student’s t-test because the former can accommodate parameters with a non-normal cumulative distribution function. This is the case for both PWV and r^2 because the ranges of these parameters are limited: PWV cannot be negative for a forward-propagating pulse wave (it is negative for a reflected wave, but in this study reflected waves were ignored), and r^2 must range between 0 and 1. In all cases, the Kolmogorov-Smirnov test returned higher p-values than the unpaired, two-sided

Student's *t*-test, indicating that the former test provides a stricter measure of significance than the latter.

Histology

Figure 6 shows examples of H&E-stained transverse sections of the aorta from a normal vessel (Figure 6a), an aneurysm (Figure 6b), and at the site of a rupture (Figure 6c and close-up in Figure 6d). Each sample was selected from a different mouse, with the rupture sample coming from the same mouse whose case history was examined in the previous section. No histology is shown for fissures because, under the definition used in this study, this designation can only be applied retroactively once an aneurysm has been observed at the same site. It should also be noted that the length scales in Figure 6 do not correspond to the dimensions in vivo; this is because the fixation process tends to shrink tissue, and because the aorta is no longer under tension or intraluminal pressure once it has been excised.

In the normal vessel (Figure 6a), the wall was found to be uniform and free of degradation. In contrast, there was visible degradation in the wall of the sac in the aneurysmal case (Figure 6b) as well as a breach in the wall of the ruptured aorta (Figures 6c and 6d). In total, histology was performed on 11 of the 18 mice (the other 7 mice died in between experimental time points; in these instances, the aorta could not be excised and preserved in time). Similar observations were made in all of these mice, with the histology in each case corresponding to the last observed disease stage (normal, aneurysmal, or ruptured) before the mouse was sacrificed.

Discussion

The primary objective of this study was to assess the capability of PWI to distinguish between the four stages of disease progression in the murine angiotensin II AAA model: normal, fissured, aneurysmal, and ruptured. Although not all animals necessarily underwent all four of these stages (either because the disease did not progress far enough, or because the stage occurred between acquisitions), the results in Figures 3-5 show that PWI can be used to identify and differentiate each stage from the others. Figures 3 and 4 demonstrate that the pulse wave pattern changes qualitatively as the aneurysm progresses through these four stages. In normal vessels, the wave propagates at a constant velocity; in AAA sacs, the wave amplitude is significantly reduced; and in fissures and ruptures, the pulse wave is absent and is replaced by high-amplitude displacements. As Figures 3 and 4 illustrate, these patterns are easily distinguished using either PWI cine-loops (Figure 3) or spatiotemporal displacement maps along the vessel wall (Figure 4).

In addition to the aforementioned qualitative disease markers, Figure 5 shows that PWI can also be used to distinguish stages of aneurysm development quantitatively by tracking changes in the velocity of the pulse wave (PWV) as well as its coefficient of determination (r^2). Figure 5a shows that the PWV is significantly higher in normal aortas than in aneurysms, while Figure 5b shows that r^2 is highest in normal vessels, significantly lower in aneurysms, and lowest in fissures and ruptures (less than 0.20). These results demonstrate that PWI provides an effective means of monitoring the progression of murine AAAs, and

that it is possible to identify the stage of AAA disease using both qualitative features and quantitative parameters associated with pulse wave propagation.

For normal aortas, the high r^2 values and the range of PWVs obtained (2.8±0.9 m/s) are consistent with the literature (Hartley et al., 1997; Wang et al., 2000; Williams et al., 2007). The lower values of r^2 in aneurysms imply that the composition of the sac walls are less homogeneous than the walls of normal vessels, which also agrees well with other studies (Challa and Han, 2007; Collins et al., 2011; Genovese et al., 2012). However, the decrease in PWV observed within the aneurysms differs from most studies, which in their majority show increased PWV in the sac wall for both murine (Barisione et al., 2006; Fujikura et al., 2007) and human (Volokh and Vorp, 2008) aneurysms, although some studies have found that the vessel walls of human aneurysms can also soften under certain conditions (Vorp et al., 1996; Long et al., 2004). The discrepancy may be caused by the increased dose of angiotensin II; as mentioned previously, the dose was set up to three times higher in this study than what has typically been reported in the literature, in order to increase the probability of fissure and rupture events. The higher dose of angiotensin II would likely have degraded the walls of the aortas faster than usual, preventing them from remodeling and stiffening as they might have under a normal dose. Moreover, the accelerated degradation of the vessel would likely have increased the presence of wall remnants and blood clots in the lumen, which may in turn have contributed to the formation of a larger and stiffer thrombus in the aneurysm sac. This would explain the observed reduction in displacement in the aneurysm sacs, since the presence of a thrombus has been shown to decrease the pressure transmitted to the vessel wall (Thubrikar et al., 2003). In future studies, mechanical testing of the aneurysm sacs could be used to test these proposed explanations.

The high displacements directed out of the lumen at fissure and rupture sites (Figures 4b and 4d) are indicative of blood leakage through gaps in the vessel wall. This explanation is corroborated by the PW Doppler measurements, which as mentioned previously showed flow rates of up to 40 cm/s at the sites of fissures and ruptures in cases where these abnormalities were visible on the B-mode during imaging. Hence, the blood leaking out of the lumen likely causes high displacements to appear in the surrounding tissue because its rate of flow is an order of magnitude faster than tissue motion (up to 40 cm/s for the blood compared to at most 10 mm/s for tissue). This explanation is also consistent with the low values of r^2 at the sites of these abnormalities, since a fissure or rupture in the vessel wall would mean that there is no pulse wave to track in the intervening space. The fact that fissures and ruptures appear similar both qualitatively (identical displacement patterns in Figures 4b and 4d) as well as quantitatively (p-value of 0.87 in Figure 5b) also agrees with these events being the same from a physical perspective, with the only difference being that the former is defined as occurring before an aneurysm forms and the latter is defined as occurring afterwards. Finally, it should be noted that in some cases, the presence of the fissure or rupture was not readily apparent on the B-mode, and was only revealed using PWI. This demonstrates that PWI can provide complementary information to that provided by standard B-mode monitoring of aneurysms, while being based on essentially the same acquired signals.

As mentioned previously, although PWI has been successfully applied in humans (Luo et al., 2012; Li et al., 2013), in this work murine aneurysms were studied as a proxy for human ones principally to enable monitoring AAA disease progression over its entire duration and at many closely spaced time-points, in addition to several other key advantages (the ability to instigate aneurysms in a controlled fashion, considerably shorter AAA development time, as well as higher spatial and temporal resolutions). However, although there are similarities between murine angiotensin II aneurysms and human ones from the perspective of PWI alone, the mechanisms that underlie the formation of these aneurysms are different: human AAAs tend to form as a result of gradual, localized wall degradation, and typically do not involve fissures in the aortic wall. Hence, while the indicators that precede aneurysm formation in the murine AAA model are those associated with a fissure (high displacements and low r^2), the analogous indicators in humans will be entirely different. Aneurysm formation in humans would most likely be preceded a localized change in peak displacement, PWV, and r^2, all of which would correspond to a local change in wall stiffness as the extracellular matrix of the vessel would begin to degrade. Nevertheless, the present work has important implications for the clinical use of PWI, in that it demonstrates that PWI can detect subtle indicators of aneurysm formation in vivo, and also suggests analogous features to look for in humans. Notably, the pulse wave patterns for normal and aneurysmal human aortas observed by Li et al. (2013) are similar to those presented here for mice (lower displacement in the wall of the sac and lower r^2). Ultimately, longitudinal clinical studies of PWI monitoring are needed to determine the precise indicators that precede aneurysm formation, and thus monitor the progression of AAA disease in humans.

Conclusions

This study demonstrates that PWI can be used to stage the progress of AAA disease in a murine model by differentiating normal aortas from those with fissures, aneurysms, and ruptures. PWV was constant in normal aortas (2.8 ± 0.9 m/s, $r^2 = 0.89 \pm 0.11$) owing to the relatively homogeneous composition of these vessels. In AAA sacs, the wave speeds were 45% lower (1.6± 0.6 m/s) and exhibited more variability ($r^2 = 0.66\pm 0.23$). Moreover, the wall displacements induced by the pulse waves were at least 80% lower within the sacs compared to the surrounding vessel. Finally, at the sites of fissures and ruptured AAAs, higher PWI wall displacements directed outwards from the lumen and with no discernible wave pattern ($r^2 < 0.20$) were observed throughout the cardiac cycle.

The findings of this study show that PWI could potentially be used to monitor the growth and propensity for rupture of human aneurysms by supplying complementary information to that provided by standard B-mode imaging.

Supplementary Material

Refer to Web version on PubMed Central for supplementary material.

Acknowledgments

The authors acknowledge funding from the National Institutes of Health (NIH R01-HL098830). The authors would like to thank Dr. Shunichi Homma for the use of the Visualsonics Vevo 770 ultrasound imager. The authors also

wish to thank Iason-Zacharias Apostolakis, Claire Chang, Ronny Li, Jianwen Luo, Fusako Sera, Danial Shahmirzadi, and Anushree Srivastava for their assistance.

References

Adji A, O'Rourke MF, Namasivayam M. Arterial stiffness, its assessment, prognostic value, and implications for treatment. American Journal of Hypertension. 2011; 241:5–17. [PubMed: 20940710]

Allison MA, Kwan K, DiTomasso D, Wright CM, Criqui MH. The epidemiology of abdominal aortic diameter. Journal of Vascular Surgery. 2008; 481:121–127. [PubMed: 18515037]

Barisione C, Charnigo R, Howatt DA, Moorleghen JJ, Rateri DL, Daugherty A. Rapid dilation of the abdominal aorta during infusion of angiotensin II detected by noninvasive high-frequency ultrasonography. Journal of Vascular Surgery. 2006; 442:372–376. [PubMed: 16890871]

Brewster DC, Cronenwett JL, Hallett JW, Johnston KW, Krupski WC, Matsumura JS. Guidelines for the treatment of abdominal aortic aneurysms. Journal of Vascular Surgery. 2003; 375:1106–1117. [PubMed: 12756363]

Challa V, Han HC. Spatial variations in wall thickness, material stiffness and initial shape affect wall stress and shape of intracranial aneurysms. Neurological Research. 2007; 296:569–577. [PubMed: 17535557]

Chiu YC, Arand PW, Shroff SG, Feldman T, Carroll JD. Determination of pulse wave velocities with computerized algorithms. American Heart Journal. 1991; 1215:1460–1470. [PubMed: 2017978]

Choksy SA, Wilmink AB, Quick CR. Ruptured abdominal aortic aneurysm in the Huntingdon district: a 10-year experience. Annals of the Royal College of Surgeons of England. 1999; 811:27–31. [PubMed: 10325681]

Collins MJ, Bersi M, Wilson E, Humphrey JD. Mechanical properties of suprarenal and infrarenal abdominal aorta: implications for mouse models of aneurysms. Medical Engineering and Physics. 2011; 3310:1262–1269. [PubMed: 21742539]

Crawford CM, Hurtgen-Grace K, Talarico E, Marley J. Abdominal aortic aneurysm: an illustrated narrative review. Journal of Manipulative and Physiological Therapeutics. 2003; 263:184–195. [PubMed: 12704311]

de Prophetis N, Armitage HV, Triboletti ED. Rupture of tuberculous aortic aneurysm into lung. Annals of Surgery. 1959; 1506:1046–1051. [PubMed: 13814980]

Eriksson A, Greiff E, Loupas T, Persson M, Pesque P. Arterial pulse wave velocity with tissue Doppler imaging. Ultrasound in Medicine and Biology. 2002; 285:571–580. [PubMed: 12079694]

Forsdahl SH, Singh K, Solberg S, Jacobsen BK. Risk factors for abdominal aortic aneurysms: a 7-year prospective study: the TromsøStudy, 1994-2001. Circulation. 2009; 11916:2202–2208. [PubMed: 19364978]

Fujikura K, Luo J, Gamarnik V, Pernot M, Fukumoto R, Tilson MD, Konofagou EE. A novel noninvasive technique for pulse-wave imaging and characterization of clinically-significant vascular mechanical properties in vivo. Ultrasonic Imaging. 2007; 293:137–154. [PubMed: 18092671]

Fung, YC. Biomechanics: circulation. 2. Springer; New York, NY, USA: 1996.

Genovese K, Collins MJ, Lee YU, Humphrey JD. Regional finite strains in an angiotensin-II induced mouse model of dissecting abdominal aortic aneurysms. Cardiovascular Engineering and Technology. 2012; 32:194–202.

Go AS, Mozaffarian D, Roger VL, Benjamin EJ, Berry JD, Borden WB, Bravata DM, Dai S, Ford ES, Fox CS, Franco S, Fullerton HJ, Gillespie C, Hailpern SM, Heit JA, Howard VJ, Huffman MD, Kissela BM, Kittner SJ, Lackland DT, Lichtman JH, Lisabeth LD, Magid D, Marcus GM, Marelli A, Matchar DB, McGuire DK, Mohler ER, Moy CS, Mussolino ME, Nichol G, Paynter NP, Schreiner PJ, Sorlie PD, Stein J, Turan TN, Virani SS, Wong ND, Woo D, Turner MB. Heart disease and stroke statistics - 2013 update: a report from the American Heart Association. Circulation. 2013; 1271:e6–e245. [PubMed: 23239837]

Hamilton PK, Lockhart CJ, Quinn CE, McVeigh GE. Arterial stiffness: clinical relevance, measurement and treatment. Clinical Science. 2007; 1134:157–170. [PubMed: 17623012]

Hartley CJ, Taffet GE, Michael LH, Pham TT, Entman ML. Noninvasive determination of pulse-wave velocity in mice. The American Journal of Physiology. 1997; 2731(Pt 2):H494–H500. [PubMed: 9249523]

Haskett D, Johnson G, Zhou A, Utzinger U, Vande Geest JP. Microstructural and biomechanical alterations of the human aorta as a function of age and location. Biomechanics and Modeling in Mechanobiology. 2010; 96:725–736. [PubMed: 20354753]

Klevay LM. Cardiovascular disease from copper deficiency: a history. Journal of Nutrition. 2000; 1302:489–492.

Korteweg DJ. Uber die Fortpflanzungsgeschwindigkeit des Schalles in Elastischen Rohren. Annals of Physical Chemistry. 1878; 51:525–537.

Kraft KA, Itskovich VV, Fei DY. Rapid measurement of aortic wave velocity: in vivo evaluation. Magnetic Resonance in Medicine. 2001; 46:95–102. [PubMed: 11443715]

Lasheras JC. The biomechanics of arterial aneurysms. Annual Review of Fluid Mechanics. 2007; 391:293–319.

Laurent S, Cockcroft J, van Bortel LM, Boutouyrie P, Giannattasio C, Hayoz D, Pannier BM, Vlachopoulos C, Wilkinson IB, Struijker Boudier HAJ. Expert consensus document on arterial stiffness: methodological issues and clinical applications. European Heart Journal. 2006; 2721:2588–2605. [PubMed: 17000623]

Lehmann ED. Clinical value of aortic pulse-wave velocity measurement. The Lancet. 1999; 3549178:528–529.

Lemaître V. Increased medial degradation with pseudo-aneurysm formation in apolipoprotein E-knockout mice deficient in tissue inhibitor of metalloproteinases-1. Circulation. 2002; 1072:333–338.

Li RX, Luo J, Balaram SK, Chaudhry FA, Shahmirzadi D, Konofagou EE. Pulse wave imaging in normal, hypertensive and aneurysmal human aortas in vivo: a feasibility study. Physics in Medicine and Biology. 2013; 5813:4549–4562. [PubMed: 23770991]

Long A, Rouet L, Bissery A, Rossignol P, Mouradian D, Sapoval M. Compliance of abdominal aortic aneurysms: evaluation of tissue Doppler imaging. Ultrasound in Medicine and Biology. 2004; 309:1099–1108. [PubMed: 15550314]

Luo J, Fujikura K, Tyrie LS, Tilson MD, Konofagou EE. Pulse wave imaging of normal and aneurysmal abdominal aortas in vivo. IEEE Transactions on Medical Imaging. 2009; 284:477–486. [PubMed: 19272985]

Luo J, Konofagou EE. A fast normalized cross-correlation calculation method for motion estimation. IEEE Transactions on Ultrasonics, Ferroelectrics and Frequency Control. 2010; 576:1347–1357.

Luo J, Li RX, Konofagou EE. Pulse Wave Imaging (PWI) of the human carotid artery: an in vivo feasibility study. The Journal of the Acoustical Society of America. 2012; 1314:174–181.

Macgowan CK, Henkelman RM, Wood ML. Pulse-wave velocity measured in one heartbeat using MR tagging. Magnetic Resonance in Medicine. 2002; 481:115–121. [PubMed: 12111938]

Manning MW, Cassis LA, Huang J, Szilvassy SJ, Daugherty A. Abdominal aortic aneurysms: fresh insights from a novel animal model of the disease. Vascular Medicine. 2002; 71:45–54. [PubMed: 12083734]

McGloughlin TM, Doyle BJ. New approaches to abdominal aortic aneurysm rupture risk assessment: engineering insights with clinical gain. Arteriosclerosis, Thrombosis, and Vascular Biology. 2010; 309:1687–1694.

Mitchell GF. Arterial stiffness and wave reflection: biomarkers of cardiovascular risk. Artery Research. 2009; 32:56–64. [PubMed: 20161241]

Moens, AI. Die Pulskurve PhD thesis. Leiden University; Leiden, The Netherlands: 1877.

Murphy SL, Xu J, Kochanek KD. Deaths: final data for 2010. National Vital Statistics Reports. 2013; 614:1–167. [PubMed: 24979972]

Nemes A, Takács R, Gavallér H, Várkonyi TT, Wittmann T, Forster T, Lengyel C. Correlations between arteriograph-derived pulse wave velocity and aortic elastic properties by echocardiography. Clinical Physiology and Functional Imaging. 2011; 311:61–65. [PubMed: 21040403]

Patterson BO, Holt PJE, Hinchliffe R, Loftus IM, Thompson MM. Predicting risk in elective abdominal aortic aneurysm repair: a systematic review of current evidence. European Journal of Vascular and Endovascular Surgery. 2008; 366:637–645. [PubMed: 18922709]

Pernot M, Fujikura K, Fung-Kee-Fung SD, Konofagou EE. ECG-gated, mechanical and electromechanical wave imaging of cardiovascular tissues in vivo. Ultrasound in Medicine and Biology. 2007; 337:1075–1085. [PubMed: 17507146]

Rabben SI, Stergiopulos N, Hellevik LR, Smiseth OA, Slø rdahl S, Urheim S, Angelsen Br. An ultrasound-based method for determining pulse wave velocity in superficial arteries. Journal of Biomechanics. 2004; 3710:1615–1622. [PubMed: 15336937]

Sakalihasan N, Limet R, Defawe OD. Abdominal aortic aneurysm. The Lancet. 2005; 365(9470): 1577–1589.

Savitzky A, Golay MJE. Smoothing and differentiation of data by simplified least squares procedures. Analytical Chemistry. 1964; 368:1627–1639.

Segers P, Georgakopoulos D, Afanasyeva M, Champion HC, Judge DP, Millar HD, Verdonck PR, Kass DA, Stergiopulos N, Westerhof N. Conductance catheter-based assessment of arterial input impedance, arterial function, and ventricular-vascular interaction in mice. American Journal of Physiology. Heart and Circulatory Physiology. 2005; 2883:H1157–H1164. [PubMed: 15604134]

Shahmirzadi D, Konofagou EE. Detection of aortic wall inclusions using regional pulse wave propagation and velocity in silico. Artery Research. 2012; 63:114–123.

Shahmirzadi D, Narayanan P, Li RX, Qaqish WW, Konofagou EE. Mapping the longitudinal wall stiffness heterogeneities within intact canine aortas using Pulse Wave Imaging (PWI) ex vivo. Journal of Biomechanics. 2013; 4611:1866–1874. [PubMed: 23764176]

Stather PW, Dattani N, Bown MJ, Earnshaw JJ, Lees TA. International variations in AAA screening. European Journal of Vascular and Endovascular Surgery. 2013; 453:231–234. [PubMed: 23332307]

Sugawara J, Hayashi K, Yokoi T, Tanaka H. Carotid-femoral pulse wave velocity: impact of different arterial path length measurements. Artery Research. 2010; 41:27–31. [PubMed: 20396400]

Sutton-Tyrrell K, Najjar SS, Boudreau RM, Venkitachalam L, Kupelian V, Simonsick EM, Havlik R, Lakatta EG, Spurgeon H, Kritchevsky S, Pahor M, Bauer D, Newman AB. Elevated aortic pulse wave velocity, a marker of arterial stiffness, predicts cardiovascular events in well-functioning older adults. Circulation. 2005; 11125:3384–3390. [PubMed: 15967850]

Thubrikar MJ, Robicsek F, Labrosse M, Chervenkoff V, Fowler BL. Effect of thrombus on abdominal aortic aneurysm wall dilation and stress. The Journal of Cardiovascular Surgery. 2003; 441:67–77. [PubMed: 12627076]

Urbonavicius S, Urbonaviciene G, Honoré B, Henneberg EW, Vorum H, Lind-holt JS. Potential circulating biomarkers for abdominal aortic aneurysm expansion and rupture - a systematic review. European Journal of Vascular and Endovascular Surgery. 2008; 363:273–280. [PubMed: 18639476]

Vappou J, Luo J, Konofagou EE. Pulse wave imaging for noninvasive and quantitative measurement of arterial stiffness in vivo. American Journal of Hypertension. 2010; 234:393–398. [PubMed: 20094036]

Volokh KY, Vorp DA. A model of growth and rupture of abdominal aortic aneurysm. Journal of Biomechanics. 2008; 415:1015–1021. [PubMed: 18255074]

Vorp DA, Raghavan ML, Muluk SC, Makaorun MS, Steed DL, Shapiro R, Webster MW. Wall strength and stiffness of aneurysmal and nona-neurysmal abdominal aorta. Annals of the New York Academy of Sciences. 1996; 8001:274–276. The Abdominal. [PubMed: 8959012]

Vorp DA, Raghavan ML, Webster MW. Mechanical wall stress in abdominal aortic aneurysm: influence of diameter and asymmetry. Journal of Vascular Surgery. 1998; 274:632–639. [PubMed: 9576075]

Walker WF, Trahey GE. A fundamental limit on delay estimation using partially correlated speckle signals. IEEE Transactions on Ultrasonics, Ferroelectrics and Frequency Control. 1995; 422:301–308.

Wang YX, Halks-Miller M, Vergona R, Sullivan ME, Fitch R, Mallari C, Martin-McNulty B, da Cunha V, Freay A, Rubanyi GM, Kauser K. Increased aortic stiffness assessed by pulse wave

velocity in apolipoprotein E-deficient mice. American Journal of Physiology: Heart and Circulatory Physiology. 2000; 2782:H428–H434. [PubMed: 10666072]

Williams R, Needles A, Cherin E, Zhou YQ, Henkelman RM, Adamson SL, Foster FS. Noninvasive ultrasonic measurement of regional and local pulse-wave velocity in mice. Ultrasound in Medicine and Biology. 2007; 339:1368–1375. [PubMed: 17561330]

Wilson JS, Virag L, Di Achille P, Karsaj I, Humphrey JD. Biochemome-chanics of intraluminal thrombus in abdominal aortic aneurysms. Journal of Biomechanical Engineering. 2013; 1352:021011. [PubMed: 23445056]

Zoungas S, Asmar RP. Arterial stiffness and cardiovascular outcome. Clinical and Experimental Pharmacology and Physiology. 2007; 347:647–651. [PubMed: 17581224]

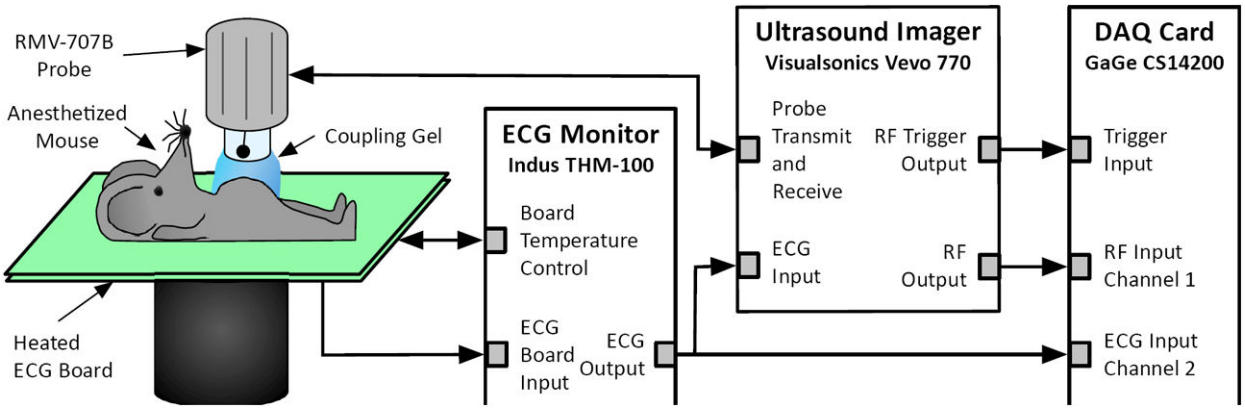

Figure 1.
Block diagram of the experimental setup.

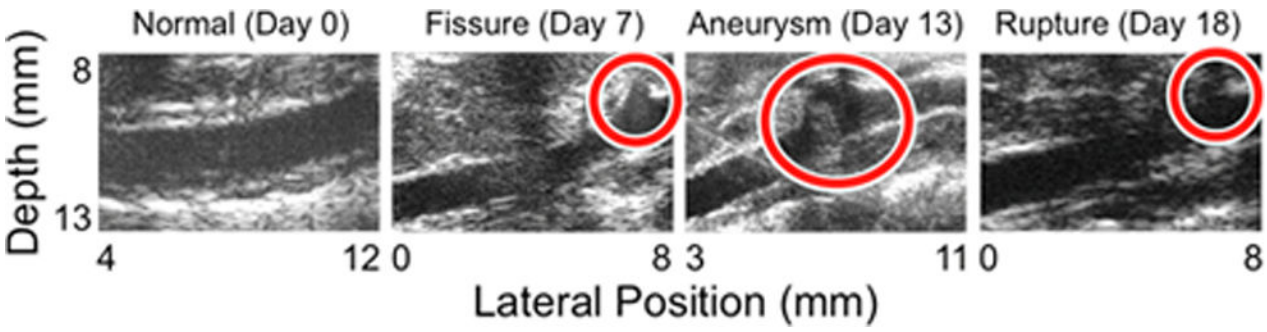

Figure 2.

B-mode images of each phase of AAA disease progression in the same mouse, showing (a) a normal aorta at day 0 (the day before angiotensin II infusion), (b) a fissure at day 7, (c) an aneurysm at day 13, and (d) a rupture at day 18. The locations of the fissure, aneurysm, and rupture are indicated with circles. PW Doppler measurements were also taken immediately outside the vessel wall in the case of the fissure and the ruptures, and within the sac of the aneurysm (approximately within the top halves of the circles overlaid on the B-modes). The lateral position axes start at different offsets in order to align the fields of view to the same anatomical landmarks; doing this shows that in the latter three images, the abnormalities corresponding to each disease stage (fissure, aneurysm, and rupture) all appear around 8 mm.

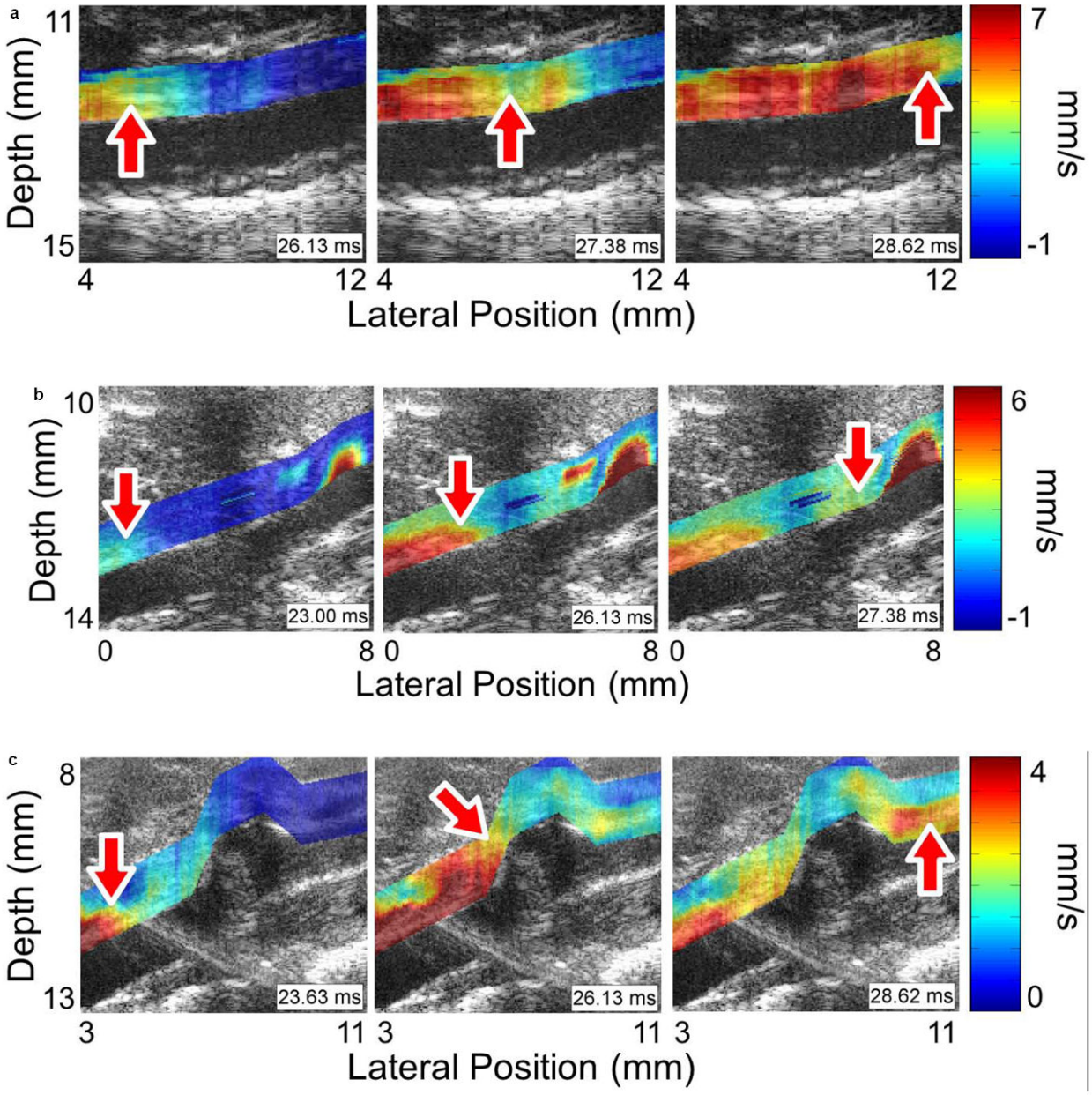

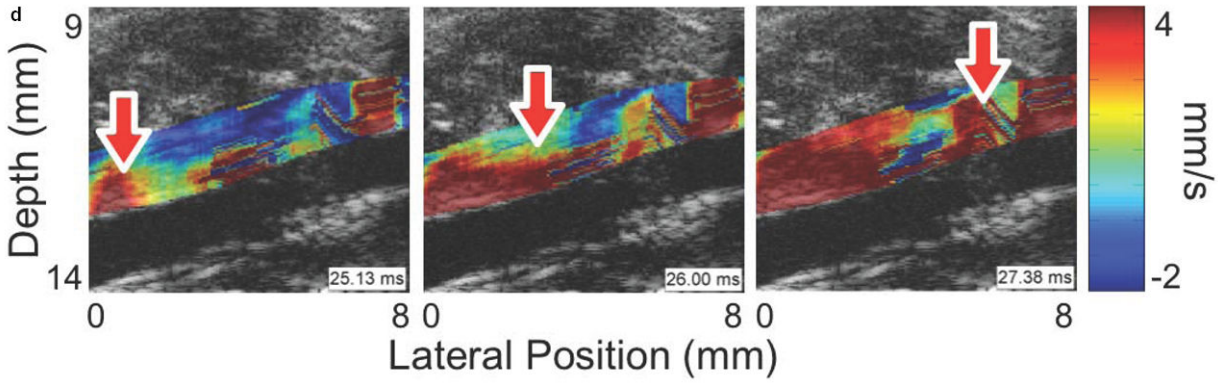

Figure 3.

Examples of pulse wave propagation visualized with PWI (B-mode frames overlaid with wall displacement) as the wave enters (left), crosses (middle), and exits (right) the field of view in (a) the normal aorta, (b) the fissure, (c) the aneurysm, and (d) the rupture shown in Figure 2. The time index indicates the time elapsed since the start of the cardiac cycle (i.e. the R-wave of the ECG). The arrow in each frame indicates the location of the 50% upstroke point of the pulse wave, which is used to track the wave and calculate its velocity. As in Figure 2, the lateral position axes start at different offsets in order to align the fields of view to the same anatomical landmarks. The full PWI cine-loops for these cases are in Supplemental Video 1.

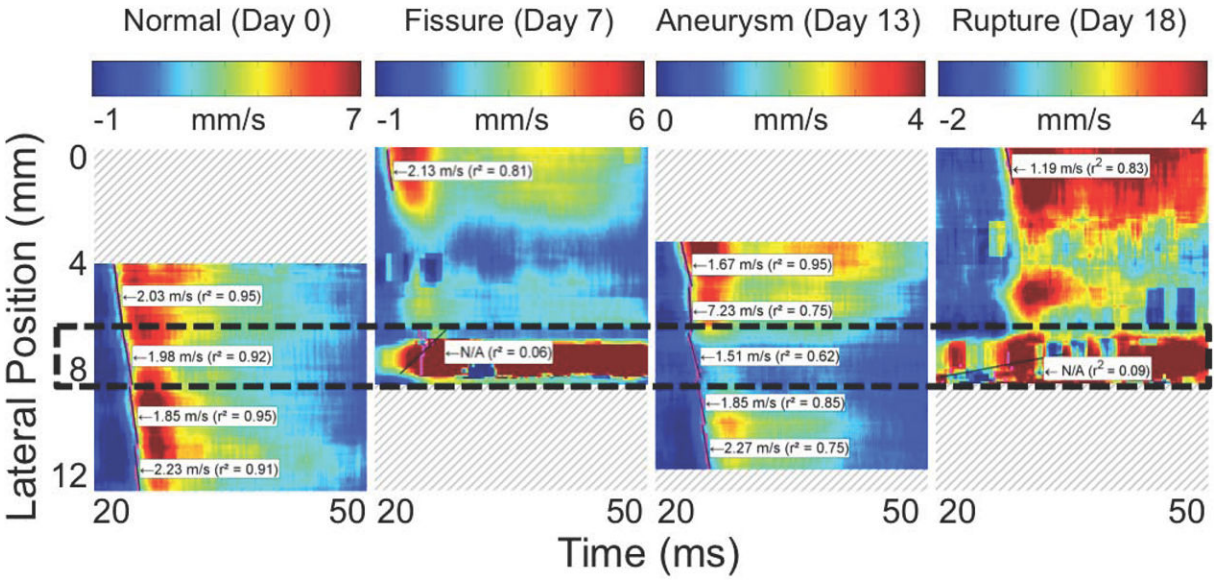

Figure 4.

Spatiotemporal maps of wall displacement in the (a) normal, (b) fissured, (c) aneurysmal, and (d) ruptured aortas shown in Figures 2 and 3. The intensity scales for each plot are the same as their respective cases in Figure 3. As in Figures 2 and 3, the lateral position axes start at different offsets in order to align the fields of view to the same anatomical landmarks. Piecewise PWV and r^2 are also shown in each case; some regions of (b) and (d) are omitted owing to noise.

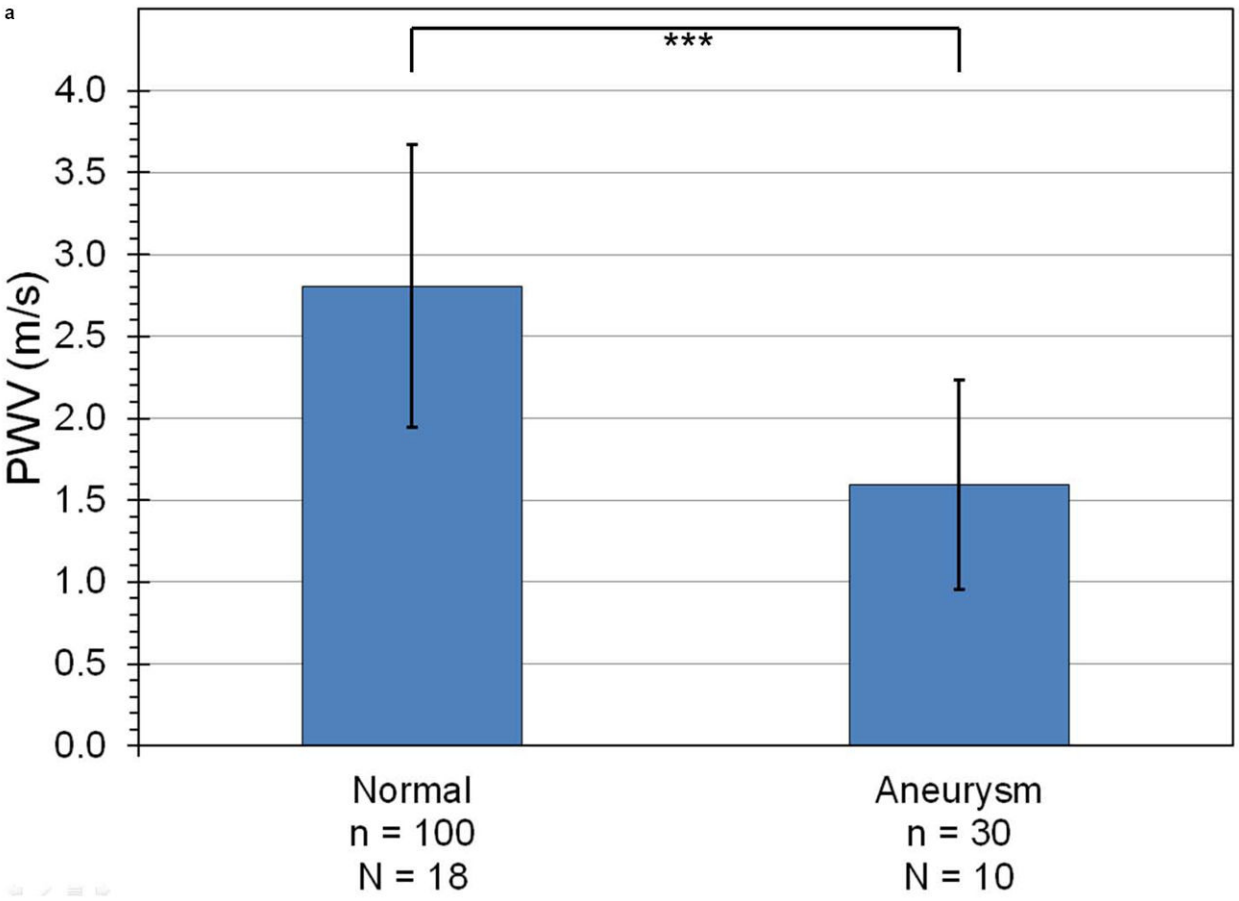

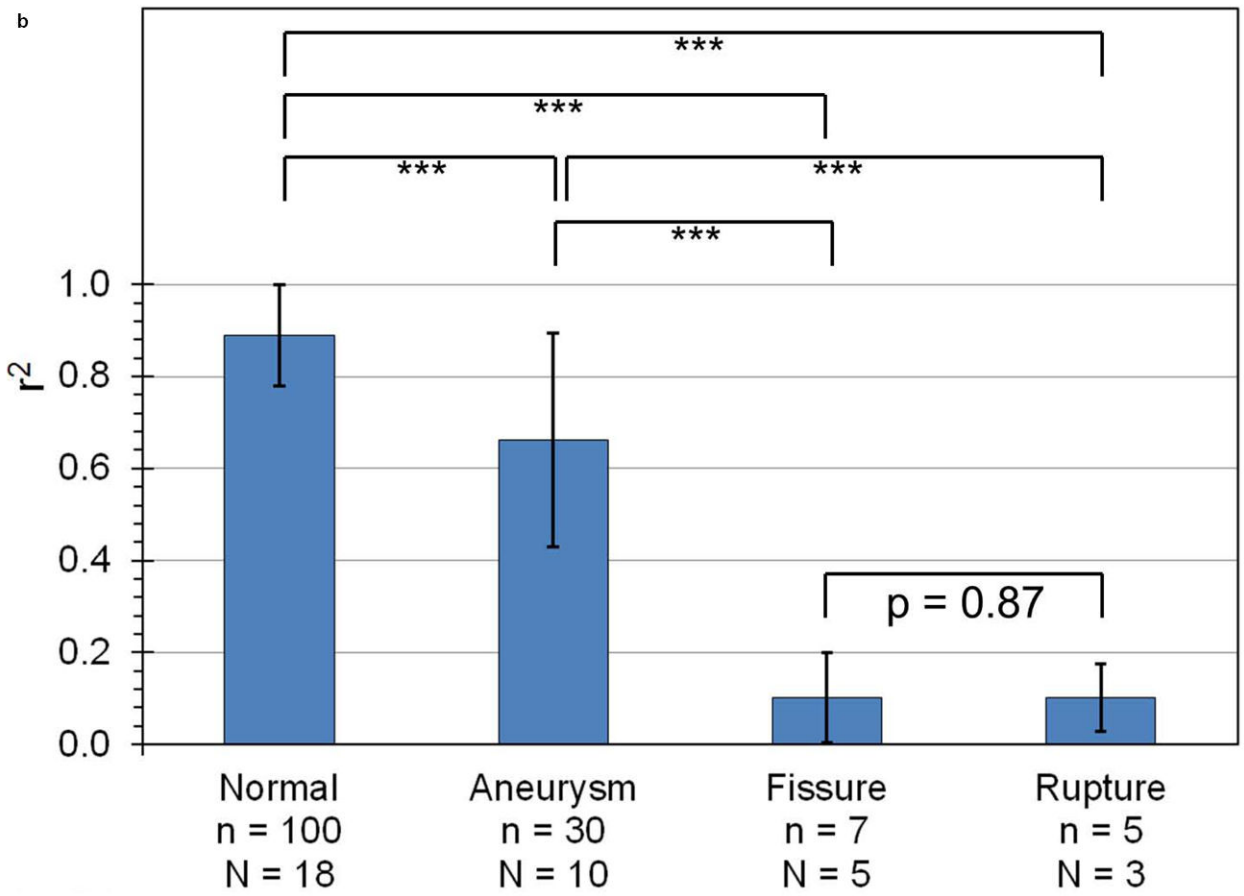

Figure 5.

Mean and standard deviation of (a) PWV and (b) r^2 for linear regressions performed on all observed cases of normal aortas, aneurysms, fissures, and ruptures. The number of acquisitions (n) and mice (N) being averaged across are also indicated. With the exception of fissures compared to ruptures, PWV and r^2 are statistically significant differentiators between any two categories ($p < 0.001$, indicated by the triple asterisk).

a

b

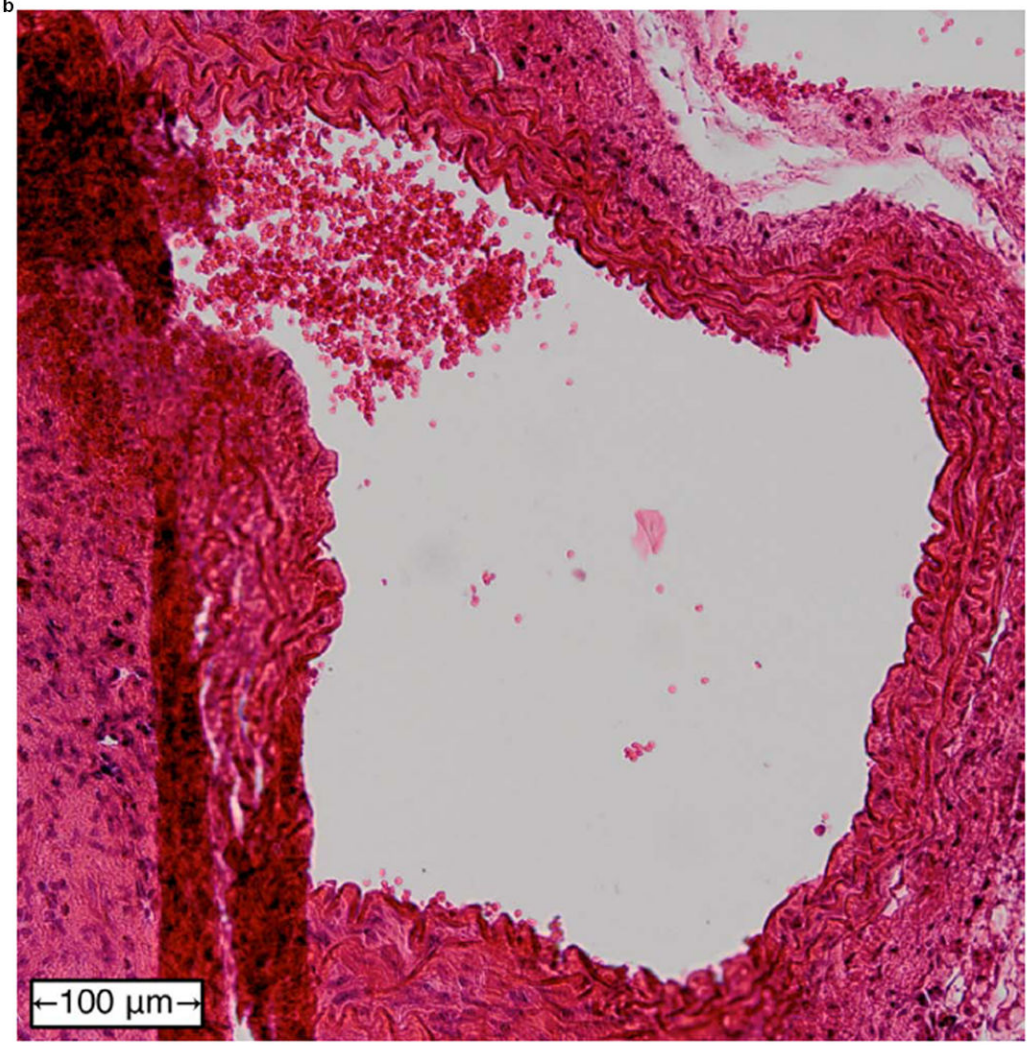

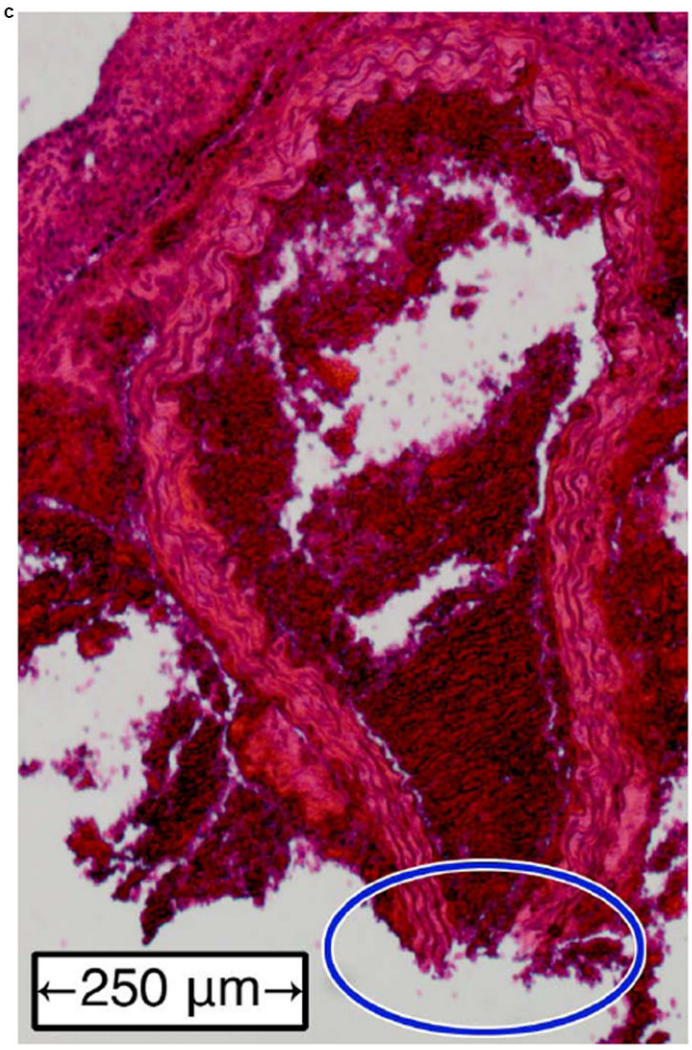

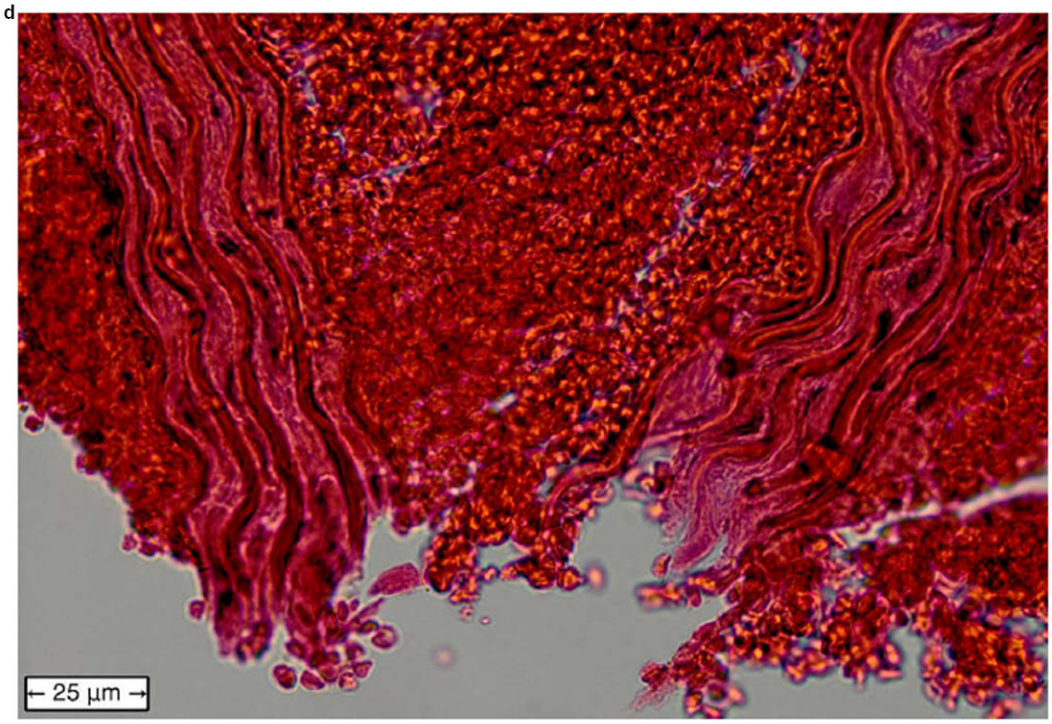

Figure 6.
Examples of H&E-stained, transverse sections of aorta for (a) a normal vessel, (b) an aneurysm with the sac at the top-left, (c) a ruptured aneurysm, and (d) a close-up of the ruptured area circled in (c).